Published in final edited form as:
Cytometry A. 2008 December ; 73A(12): 1116–1127. doi:10.1002/cyto.a.20667.

Very Small Embryonic- Like stem cells (VSELs) are present in adult murine organs: ImageStream based morphological analysis and distribution studies

Ewa K. Zuba-Surma[a,*], **Magdalena Kucia**[a], **Wan Wu**[a], **Izabela Klich**[a], **James W. Lillard Jr.**[b], **Janina Ratajczak**[a], and **Mariusz Z. Ratajczak**[a,*]

[a]Stem Cell Biology Institute, University of Louisville, Louisville, KY, USA

[b]Brown Cancer Center, University of Louisville, Louisville, KY, USA

Abstract

Recently, we purified a population of CXCR4$^+$/Oct-4$^+$/SSEA-1$^+$/Sca-1$^+$/Lin$^-$/CD45$^-$ Very Small Embryonic-Like stem cells (VSELs) from adult murine bone marrow (BM). After employing flow cytometry, ImageStream analysis, confocal microscopy, and real time RT-PCR, we report that similar cells could be also identified and isolated from several organs in adult mice. The highest total numbers of Oct-4$^+$ VSELs were found in the brain, kidneys, muscles, pancreas, and BM. These observations support our hypothesis that a population of very primitive cells expressing germ line/epiblast markers (Oct-4, SSEA-1) is deposited early during embryogenesis in various organs and survives into adulthood. Further studies are needed to determine whether these cells, after being isolated from various adult human organs similarly to their murine BM-derived counterparts, are endowed with pluripotent stem cell properties.

Keywords

VSELs; Oct-4; CXCR4; pluripotent stem cells; ImageStream

INTRODUCTION

Adult bone marrow (BM) tissue has been considered a “home” of various types of primitive cells for many years (1,2). As a result of these studies, several types of nonhematopoietic stem cells (HSCs) have been described in adult BM, including: i) endothelial progenitor cells (EPCs) (3,4) ii) mesenchymal (M)SCs (5,6); iii) multipotent adult (MA)PCs (7); and iv) marrow-isolated adult multilineage inducible (MIAMI) cells (8) as well as precursors of germ cells (oocytes and spermatogonial cells) (9,10). The presence of multiple populations of SCs in the BM could potentially be a result of the “developmental migration” of SCs during ontogenesis as well as the presence of the permissive environment that attracts these cells to the BM.

Recently, our group purified a population of developmentally primitive SCs from BM that we named very small embryonic-like SCs (VSELs) (11). These rare cells were isolated by

Address for correspondence: Mariusz Z. Ratajczak M.D., Ph.D. or Ewa K. Zuba-Surma, Ph.D., Stem Cell Institute, James Graham Brown Cancer Center, University of Louisville, 500 Floyd St., Louisville, KY 40202, Telephone: (502) 852-3486, Fax: (502) 852-3032, E-mail: mzrata01@louisville.edu or ekzuba01@louisville.edu.

Based on the work presented in this manuscript, the first author was awarded the ISAC President’s Award of Excellence at the ISAC Meeting in Budapest (May 2008).

multiparameter fluorescent activated cell sorting (FACS) as a population of Sca-1^+/Lin^-/$CD45^-$ cells. Using transmission electron microscopy (TEM), we observed that these VSELs contain relatively large nuclei filled with a primitive type of chromatin (11). Further analysis employing the ImageStream system (ISS) confirmed the particularly small size (<5μm) of BM-derived VSELs as well as a high nuclear-to-cytoplasmic (N/C) ratio, thus indicating their primitive characteristics (12). We have also found VSELs are enriched in multiple tissue-specific markers, including early skeletal muscle, heart muscle, neural, liver, intestinal epithelium, and skin epidermis as well as endocrine pancreas markers. We confirmed their pluripotency by demonstrating their ability to differentiate into cellular lineages from all three germ-layers *in vitro* (11,13,14).

Moreover, we have also demonstrated that BM-derived VSELs express a multitude of markers characterizing pluripotent (P)SCs of developing epiblasts such as SSEA-1, Oct-4, Nanog, and Rex-1 (11). We hypothesize that VSELs are descendants of epiblast-derived (EP)SCs that were deposited in the BM and other organs in the early stages of development (15,16). Of note, the presence of cells possessing very small size (<5 μm) in adult murine tissues has been postulated by several investigators (17-20).

In this study, we wished to determine whether cells with the VSEL phenotype (small Oct-4^+/Sca-1^+/Lin^-/$CD45^-$ cells) could also be detected in other adult murine tissues and organs. To test this hypothesis, we employed classical flow cytometry (FCM) supported by ISS. ISS is a multispectral imaging flow cytometer allowing statistical analysis and imaging of cells acquired in suspension. We found ISS to be a useful supportive tool for flow cytometry that provides direct visualization of these acquired objects (“decoding dot”). With ISS, we are able to clearly distinguish between truly positive cells and falsely positive artifacts or debris. This is particularly important for analyses of very small cells (such as VSELs) to distinguish them from large platelets and cell debris while analyzing material isolated from homogenized solid tissues. By employing ISS for this study, we investigated the presence of Sca-1^+/Lin^-/$CD45^-$ cells in adult tissues and estimated a number of Oct-4^+ cells among populations of putative VSELs. Furthermore, we evaluated basic morphological features of these cells such as their size and N/C ratio, which are parameters related to the primitive nature of SCs.

MATERIAL AND METHODS

Animals

These experiments were performed in accordance with the guidelines set forth by the University of Louisville’s Institutional Animal Care and Use Committee (IACUC). The investigation conforms to the Guide for the Care and Use of Laboratory Animals published by the US National Institutes of Health (NIH Publication No. 85-23, revised 1996).

Isolation of cells for flow cytometric analysis

Organs of adult C57BL/6 mice (4-8 weeks old) (Jackson Laboratory, Bar Harbor, ME) were harvested after whole body perfusion with phosphate buffered saline (PBS) (Invitrogen, Carlsbad, CA). Brain, heart, skeletal muscles, pancreas, lungs, testis, kidneys, spleen, thymus, and liver were mechanically fragmented and enzymatically digested with collagenase I and collagenase II solution (both 1mg/ml; Sigma Aldrich, St. Louis, MO) for 30 to 60 min in 37°C. For liver digestion, collagenase IV (1mg/ml; Sigma Aldrich) was additionally used. Neurosensory retina (NSR) and retinal pigment epithelium (RPE) were obtained from eye tissues by enzymatic digestion as described (21). The following enzymes were used for digestion: 0.25% trypsin with 1 mM EDTA (Invitrogen); collagenase I (0.5%; Invitrogen); and hyaluronidase (0.05%; Invitrogen) for 1 hr each at 37°C.

Cell suspensions were collected, filtered through a 70 μm strainer, washed, and resuspended in medium RPMI with 2% fetal bovine serum (FBS; Invitrogen). BM was flushed from tibias and femurs without enzymatic digestion. BM after isolation as well as the suspension of cells derived from spleen and lungs were additionally treated with 1xBD Pharm Lyse Buffer (BD Pharmingen, San Jose, CA) to remove red blood cells. Cells were washed and resuspended in full medium (RPMI with 2% FBS).

Staining followed by flow cytometric analysis was performed in medium containing 2% FBS. The following anti-mouse antibodies detecting CD45, lineage markers (Lin), and Sca-1 expression (BD Pharmingen) were employed in the staining: rat anti-CD45 (APC-Cy7, clone 30-F11); anti-CD45R/B220 (PE, clone RA3-6B2); anti-Gr-1 (PE, clone RB6-8C5); anti-TCRαβ (PE, clone H57-597); anti-TCRγδ (PE, clone GL3); anti-CD11b (PE, clone M1/70); anti-Ter119 (PE, clone TER-119); and anti-Ly-6A/E (Sca-1) (FITC, clone E13-161.7). Cells were then washed, fixed with 4% paraformaldehyde for 20 min, and permeabilized with 0.1% Triton X-100 solution for 10 min. Stained cells were resuspended in PBS for further analysis and 7-aminoactinomycin D (7-AAD; Invitrogen, Molecular Probes; 40μM) was added to stain nucleated objects.

The content of $Sca\text{-}1^+/Lin^-/CD45^-$ cells was estimated among nucleated, $7\text{-}AAD^+$ events by analysis with MoFlo cell sorter (Dako, Carpintera, CA). Cells were analyzed according to the gating strategy presented in Figure 1, **Panels A and B**. The total number of cells harvested from each organ was calculated in the presence of trypan blue and was applied to compute the absolute numbers of $Sca\text{-}1^+/Lin^-/CD45^-$ and $Oct\text{-}4^+/Sca\text{-}1^+/Lin^-/CD45^-$ cells present in each analyzed organ.

ImageStream system analysis

Cells derived from different organs were isolated from adult C57BL/6 mice as described above for flow cytometric analysis. To investigate the presence of $Sca\text{-}1^+/Lin^-/CD45^-$ cells in analyzed organs, cells were stained for CD45, Lin, and Sca-1 antigen. Based on the detection channels available in the ISS, the following anti-mouse antibodies (BD Pharmingen) were employed for staining: anti-CD45R/B220 (PE, clone RA3-6B2); anti-Gr-1 (PE, clone RB6-8C5); anti-TCRαβ (PE, clone H57-597); anti-TCRγδ (PE, clone GL3); anti-CD11b (PE, clone M1/70); anti-Ter119 (PE, clone TER-119); and anti-Ly-6A/E (Sca-1) (FITC, clone E13-161.7). Staining for CD45 was performed with rat anti-CD45 (PE-Cy5, clone 30-F11; eBioscience, San Diego, CA). Cells were washed after staining, fixed with 4% paraformaldehyde for 20 min, and then permeabilized with 0.1% Triton X-100 solution for 10 min. Stained cells were resuspended in PBS for further analysis. 7-AAD (Invitrogen; Molecular Probes; 40μM) was added for 5 min before analysis and samples were run directly on ISS 100 (Amnis Corporation, Seattle, WA) and analyzed as shown in Figure 1, **Panel C**.

For intranuclear Oct-4 detection and identification of the $Oct\text{-}4^+/Sca\text{-}1^+/Lin^-/CD45^-$ population, freshly isolated cells were initially fixed with 4% paraformaldehyde for 20 min and then permeabilized with 0.1% Triton X-100 solution for 10 min. Cells were washed and incubated in the presence of 10% donkey serum (Jackson Immunoresearch, West Grove, PA) to block the sites of nonspecific binding of secondary antibodies and then stained with primary anti-murine Oct-4 antibody (mouse monoclonal IgG; Chemicon Int., Temecula, CA; 1:200) for 2 hr at 37°C. Secondary antibody conjugated with FITC (polyclonal donkey anti-mouse IgG; Jackson Immunoresearch) was added following washing. Cells were incubated for 2 hr at 37°C. Following the staining for Oct-4, cells were incubated with directly conjugated antibodies against Sca-1 (PE-Cy5), CD45 (PE), and Lin (PE). Stained cells were resuspended in PBS for further analysis. 7-AAD was added for 5 min before analysis and samples were run directly on ISS 100.

Signals from FITC, PE, 7-AAD, and PE-Cy5 were detected by channels 3, 4, 5, and 6, respectively, while side scatter and brightfield images were collected in channels 1 and 2, respectively. Morphological feature of cells such as size and N/C ratio were calculated using images of cells by IDEAS software. Size was calculated based on brightfield images of cells as the length of the minor cellular axis expressed in micrometers, while the N/C ratio was computed based on brightfield cellular images and nuclear images as a ratio between the area of cytoplasm and the area of the nucleus.

Confocal microscopic analysis

Sca-1^+/Lin^-/$CD45^-$ cells, freshly sorted from various tissues, were plated for 24 hr on 22-mm-diameter plates coated with poly-L-lysine then fixed with 4% paraformaldehyde solution for 20 min. Following fixation, cells were permeabilized with 0.1% Triton X-100 (Sigma Aldrich) for 5 min. Before staining with specific antibodies, samples were blocked with 10% donkey serum (Jackson Immunoresearch) for 30 min at room temperature to avoid non-specific binding. Cells were then incubated with primary antibodies against Oct-4 (1:200, mouse monoclonal IgG; Chemicon Int.) and CD45 (1:100, rat monoclonal IgG1, clone 30-F11; BD Pharmingen) for 2 hr at 37°C. Cells were washed with PBS followed by the addition of donkey anti-mouse IgG (TRITC-conjugated) and donkey anti-rat IgG (Cy5-conjugated) secondary antibodies (Jackson Immunoresearch) at a concentration of 1:200 for 2 hr at 37°C. Cells were further incubated with anti-Sca-1 antibody (FITC-conjugated; BD Pharmingen) following cell washing after staining with secondary antibodies. Nuclei were stained with DAPI (Molecular Probes, Carlsbad,CA) for 10 minutes at 37°C. All immunofluorescence photomicrographs were acquired using a Zeiss LSM 510 confocal microscope (Carl Zeiss, Thornwood, NY).

Expression of mRNA for Oct-4 in sorted Sca-1^+/Lin^-/$CD45^-$ by RT-PCR and real time RT-PCR

RT-PCR—Total RNA was isolated from sorted Sca-1^+/Lin^-/$CD45^-$ cells derived from all analyzed organs using the RNeasy Mini Kit (Qiagen Inc., Valencia, CA). The mRNA (10 ng) was reverse-transcribed with One Step RT-PCR (Qiagen Inc.) according to the manufacturer's instructions. The resulting cDNA fragments were amplified using HotStarTaq DNA Polymerase (Qiagen Inc.). Oct-4 mRNA was detected in sorted Sca-1^+/Lin^-/$CD45^-$ cells by employing following primers-5'-ACA TCG CCA ATC AGC TTG G-3' (forward primer) and 5'-AGA ACC ATA CTC GAA CCA CAT CC-3' (reverse primer). The correct size of PCR products (51 bp) was confirmed by separation on agarose gel when compared to DNA Ladder (Invitrogen, Carlsbad, CA).

Real time RT-PCR—For real time RT-PCR analysis of Oct4 mRNA levels, total RNA was isolated from sorted Sca-1^+/Lin^-/$CD45^-$ cells with the RNeasy Mini Kit (Qiagen Inc.). The mRNA was reverse-transcribed with TaqMan Reverse Transcription Reagents (Applied Biosystems, Foster City, CA). Random hexamers were employed for this reaction. Detection of Oct-4 and β2-microglobulin (control) mRNA levels was performed by real time RT-PCR using an ABI PRISM® 7000 Sequence Detection System (Applied Biosystems). A 25 μl reaction mixture contained 12.5 μl SYBR Green PCR Master Mix, 10 ng of cDNA template, and forward and reverse primers – for Oct-4: 5'-TTC TCA ATG CTA GTT CGC TTT CTC T-3'; 5'-ACC TTC AGG AGA TAT GCA AAT CG-3' or β2-microglobulin: 5'-CAT ACG CCT GCA GAG TTA AGC A-3'; 5'-GAT CAC ATG TCT CGA TCC CAG TAG-3' (11). The threshold cycle (Ct), i.e., the cycle number at which the amount of amplified gene of interest reached a fixed threshold, was subsequently determined. Relative quantification of Oct-4 mRNA expression was calculated using the comparative Ct method. The relative quantization value of the target, normalized to an endogenous control β2-microglobulin gene and relative to a calibrator, is expressed as $2^{-\Delta\Delta Ct}$ (fold difference), where ΔCt = Ct of target

genes - Ct of endogenous control gene, and ΔΔCt = ΔCt of samples for target gene - ΔCt of calibrator for the target gene.

To avoid the possibility of amplifying contaminating DNA, five preventative measures were taken. First, all the primers for real time RTR-PCR were designed with an intron sequence inside the cDNA to be amplified. Second, all reactions were performed with appropriate negative controls (template-free controls). Third, a uniform amplification of the products was re-checked by analyzing the melting curves of the amplified products (dissociation graphs). Fourth, the melting temperature (Tm) was 57–60°C and the product Tm was at least 10°C higher than primer Tm. Finally, gel electrophoresis was performed to confirm the correct size of the amplification and the absence of unspecific bands.

Statistical Analysis

Data are expressed as mean ± SEM. The P value <0.05 was considered statistically significant. All statistical analyses were performed using the Origin (version 5.0) statistical software (Microcal Software, Inc., Northampton, MA).

RESULTS

Sca-1$^+$/Lin$^-$/CD45$^-$ cells are detectable in several adult murine organs

To analyze adult organs for the presence of Sca-1$^+$/Lin$^-$/CD45$^-$ cells, mice were perfused to remove VSELs circulating in peripheral blood. Removed organs were enzymatically homogenized and subsequently isolated nucleated cells were washed and stained with specific antibodies for FCM and ISS analysis. Flow cytometric analyses were performed on freshly isolated or fixed cells co-stained with nuclear DNA-binding dye 7-AAD (Figure 1, **Panels A** and **B,** respectively). Inclusion of 7-AAD into the staining protocol of fixed cells allowed us to visualize nucleated events. Figure 1, **Panel A** shows a representative example of flow cytometric analysis of cells freshly isolated from the thymus. Region R1 (left plot) contains all objects larger than 2μm in size (cut-off for microparticles and platelets), which are further analyzed for CD45 and hematopoietic lineage markers (Lin) expression (middle plot). Lin$^-$/CD45$^-$ cells that are present in Region R2 are subsequently analyzed for Sca-1 expression. Sca-1$^+$/Lin$^-$/CD45$^-$ cells are present in Region R3 (right plot). Figure 1, **Panel B** shows an example of the analysis performed on fixed cells isolated from thymus stained with nuclear dye. Because of fixation followed by staining with 7-AAD, only events containing DNA were included for further analysis (Region R1). 7-AAD$^+$ objects were further visualized based on their CD45 and Lin expression and only Lin$^-$ CD45$^-$ objects from Region R2 and further were characterized for expression of Sca-1 (Figure 1, **Panel B**). Sca-1$^+$/Lin$^-$/CD45$^-$ cells identified by classical FCM are shown in R3 (Figure 1, **Panels A** and **B**).

Similar analyses of fixed cells stained with 7-AAD were performed by employing the ISS analyzer (Figure 1, **Panel B**). We employed ISS to verify the results obtained from classical FCM analysis to better visualize events of interest. Based on the morphological features of acquired objects and their direct microscopical visualization by ISS, we excluded debris and artifacts while only nucleated, intact cells were selected for further analyses (Figure 1, **Panel B**).

Figure 2 and Table 1 show that after employing classical FCM and ISS, all analyzed organs were found to contain populations of Sca-1$^+$/Lin$^-$/CD45$^-$ cells. Furthermore, inclusion of nuclear dye (7-AAD) into the staining protocol significantly improved the specificity of our analysis by distinguishing nucleated objects from anucleated 7-AAD-negative debris. Figure 2 shows that classical flow cytometric analysis without 7-AAD staining to visualize nuclei in fixed cells overestimates the number of potential VSELs in adult organs. Used first, ISS

allowed visualization of acquired objects by showing their real images, which gave us opportunity to not only distinguish nucleated objects from anucleated debris, but also to separate positive cells from falsely positive artifacts. Examples of cell debris that were falsely scored by FCM as "cells" are shown in Figure 3.

Based on this, we employed ISS analysis as the most reliable method in our studies to calculate a percentage of Sca-1^+/Lin^-/$CD45^-$ cells in various murine organs (Figure 2 and Table 1). We found that brain, pancreas, and kidneys are the organs with the highest percentage content of these cells (0.947 ±0.215, 0.943 ±0.166, and 0.644 ±0.149%, respectively), while BM, spleen, and thymus possess their lowest content (0.006 ±0.001, 0.005 ±0,002, and 0.006 ±0.001%, respectively). However, when the absolute numbers of Sca-1^+/Lin^-/$CD45^-$ cells per organ were calculated, we found brain, kidneys, and lungs have the highest content of these cells (378.52 ±106.60, 228.50 ±23.30, and 81,22 ±4.93 × 10^3, respectively) and that NSR, RPE, and spleen are tissues with the lowest content of Sca-1^+/Lin^-/$CD45^-$ cells (2.14 ±0.31, 3.17 ±1.06, and 3.86± 0.43 × 10^3, respectively) (Figure 2 and Table 1).

Next, by employing ISS, we also achieved a more detailed morphological characterization of Sca-1^+/Lin^-/$CD45^-$ cells identified in different murine organs by evaluating cell size and N/C ratio (Table 1). We found that the smallest size Sca-1^+/Lin^-/$CD45^-$ cells are present in the BM and thymus (3.63 ±0.27 and 5.40 ±1.13μm, respectively), while the largest are in the liver, testes, and pancreas (8.40 ±0.17, 7.83 ±0.32, and 7.67 ±0.08 μm, respectively) (Table 1). Moreover, Sca-1^+/Lin^-/$CD45^-$ cells isolated from testes and spleen as well as BM exhibited the highest N/C ratio (2.07 ±0.30, 1.51 ±0.02 and 1.47 ±0.17, respectively), while cells from the RPE, pancreas, and liver had the lowest N/C ratio (0.84 ±0.19, 0.91 ±0.04, and 0.91 ±0.10, respectively) (Table 1). The testes were the only organ containing Sca-1^+/Lin^-/$CD45^-$ cells characterized as large cells (7.83 ±0.32μm) with a high N/C ratio (2.07 ±0.30) (Table 1).

ISS analysis of a group of Oct-4^+ cells among Sca-1^+/Lin^-/$CD45^-$ cells in adult organs

VSELs isolated from murine BM are an Oct-4 positive subpopulation of Sca-1^+ Lin^- $CD45^-$ cells. Thus, in the next step, we evaluated a number of Oct-4^+/Sca-1^+/Lin^-/$CD45^-$ cells (VSELs) in murine organs. ISS analysis was selected again as the most accurate method and cells isolated from enzymatically treated tissues were stained for Oct-4, Sca-1, CD45, and hematopoietic Lin following their fixation and staining with 7-AAD. We detected the presence of small-nucleated Oct-4^+/Sca-1^+/Lin^-/$CD45^-$ cells in all analyzed organs and tissues (Figure 4 and Table 2). We found that pancreas, brain, skeletal muscles, and kidneys are the organs with the highest percent content of these cells (0.330 ±0.099, 0.110 ±0.027, 0.082 ±0.018, and 0.056 ±0.004%, respectively), while BM, thymus, and spleen contain the lowest percentage of these Oct-4^+ cells (0.0018 ±0.0003, 0.0018 ±0.0003, and 0.005 ±0.001%, respectively) (Figure 4 and Table 2).

Next, we calculated the absolute number of these cells/ organ (Figure 5, Table 2). We found that the highest number of small-nucleated Oct-4^+/Sca-1^+/Lin^-/$CD45^-$ cells is in the brain, kidneys, skeletal muscles, pancreas, and BM (43.97 ±12.38, 19.87 ±2.03, 15.18 ±6.79, 9.41 ±4.71, and 8.39 ±2.00 × 10^3, respectively). On the other hand, heart, thymus, testes, and spleen contained the lowest numbers of these cells (1.35 ±0.56, 2.03 ±0.37, 2.38 ±1.25, and 3.86 ±0.43 × 10^3, respectively) (Figure 5 and Table 2).

Further morphological analysis of Oct-4$^+$/Sca-1$^+$/Lin$^-$/CD45$^-$ cells derived from adult organs by ISS and confocal microscopy

By employing ISS, we identified Oct-4$^+$ cells corresponding phenotypically to VSELs in various adult organs (Figure 6). ISS allowed us to distinguish Oct-4$^+$/Sca-1$^+$/Lin$^-$/CD45$^-$ VSELs from cellular debris and artifacts commonly present in enzymatically digested samples. In the next step, we employed collected images of these cells to calculate their morphological features such as average size and N/C ratio, which were computed based on brightfield and nuclear images of cells (Figure 7 and Table 2). We noticed that the smallest Oct-4$^+$/Sca-1$^+$/Lin$^-$/CD45$^-$ cells reside in the BM and heart (3.78 ±0.64 and 4.74 ±0.93 μm, respectively). At the same time, Oct-4$^+$/Sca-1$^+$/Lin$^-$/CD45$^-$ cells detected in other organs were also small (<6μm) (Figure 7 and Table 2). Furthermore, the relatively high N/C ratio confirmed the primitive character of the analyzed populations (Figure 7 and Table 2). BM and testes were identified as organs containing Oct-4$^+$/Sca-1$^+$/Lin$^-$/CD45$^-$ cells with the highest N/C ratio (2.12 ±0.33 and 2.11 ±0.40, respectively). Cells with a lower N/C ratio were observed in all other organs (Figure 7 and Table 2). However, the average N/C ratio of Oct-4$^+$ VSELs was always higher then Sca-1$^+$/Lin$^-$/CD45$^-$ populations detected in the same organs (Tables 1 and 2).

The presence of small Oct-4$^+$/Sca-1$^+$/Lin$^-$/CD45$^-$ cells detected by ISS was subsequently confirmed by confocal microscopy on Sca-1$^+$/Lin$^-$/CD45$^-$ cells sorted from various organs (Figure 8). We identified small (<5μm) Oct-4$^+$ cells with the VSEL phenotype in all organs tested (Figure 8). Furthermore, Oct-4 expression was also confirmed at the mRNA level by employing normal RT-PCR and qRT-PCR performed on sorted cells (Figure 9, **Panels A** and **B,** respectively). qRT-PCR analysis revealed a highest number of Oct-4 mRNA transcripts in Sca-1$^+$/Lin$^-$/CD45$^-$ cells isolated from BM (Figure 9, **Panel B**).

DISCUSSION

Mounting evidence reveals that in addition to monopotent tissue committed SCs, adult organs harbor populations of more primitive pluripotent/multipotent SCs. These cells have been also variously described in the literature as MAPCs, MIAMI cells, multipotent adult (MA)SCs, OmniCytes, and VSELs. It is possible that all these primitive cells described in adult tissues and isolated by different experimental approaches are in fact overlapping and/or related populations of SCs that were given different names based on circumstance (22,23). These developmentally primitive cells could be a potential back-up source for tissue committed SCs. They reside in adult tissues and are probably activated or recruited during stress or tissue injuries in attempts to regenerate damaged organs.

VSELs are a population of very small CXCR4$^+$/Oct-4$^+$/SSEA-1$^+$/Sca-1$^+$/Lin$^-$/CD45$^-$ cells that our group recently purified at the single cell level from adult murine BM. Herein, we demonstrate that very small Sca-1$^+$/Lin$^-$/CD45$^-$ cells expressing similarly as VSEL Oct-4s reside in several adult murine tissues and organs. To detect these cells in adult tissues, we employed a multidimensional methodological approach including FCM, ISS, confocal microscopy, and RT-PCR. Using classical flow cytometry supported by ISS, we estimated the content of Sca-1$^+$/Lin$^-$/CD45$^-$ cells in different organs including BM, spleen, thymus, brain, lungs, kidneys, pancreas, testes, heart, and skeletal muscles as well as in cellular layers isolated from the eye. The ISS we employed in our studies is a novel tool allowing analyses of cells in flow in suspension that combines the statistical power of large sample size analysis common for flow cytometry with the morphological features obtained by microscopic methods (24-26). The ability of this system to microscopically visualize objects acquired by cytometer allows for their verification as true or false cellular events. ISS analysis allowed us to also characterize basic morphological features of Oct-4$^+$/Sca-1$^+$/Lin$^-$/

CD45$^-$ cells harvested from different organs, including their mean cellular size and N/C ratio, which are indicators of the stemness of primitive cells.

Since VSELs circulate at low levels in peripheral blood, as we reported recently (27,28), all animals employed in our studies were perfused before organ extraction to remove cells from the blood vessels. Organs were homogenized by enzymatic or mechanical digestion. To avoid the contamination of analyzed cell suspensions by anucleated debris released during homogenization, following staining, the cells were fixed and their nuclei stained with DNA binding dye (7-AAD). Only those objects to incorporate the dye were included in further analyses (Figure 1, **Panel B**). Visualization of nuclei revealed that the number of VSELs per organ could be overestimated due to contamination by anucleated cell debris if classical FCM analysis without nuclear staining was solely employed. Therefore, flow cytometric analysis differs in its estimation of a number of VSELs depending on whether the analysis was performed on freshly isolated-or on fixed and 7-AAD-stained cells. Interestingly, the ISS analysis we employed widely in our studies corresponded better with the data obtained by FCM analysis on fixed and 7-AAD stained cells for several tissues (Figure 2). There were, however, some discrepancies based on ISS allowing visualization of all acquired objects and the exclusion of erroneous artifacts scored positively by FCM as positive events. Such events that mimic intact cells could actually be conglomerates of cell debris (result of tissue digestion) that accidentally express a panel of “positive markers” during flow cytometric analysis (Figure 3).

Therefore, positive quantity data obtained by ISS analyses are typically lower for all organs as compared to FCM because of this exclusion of falsely “positive” objects. The differences in obtained results are the highest for tissues that required using more complex enzyme mixtures for their digestion, such as RPE and NSR. The values obtained with the ISS are also lower for other digested organs including kidneys, lungs, and liver. However, the content of Sca-1$^+$/Lin$^-$/CD45$^-$ cells in enzymatically digested muscle tissues (heart and skeletal muscles) as well as BM, thymus, and testis, which were only mechanically meshed, was similar by employing fixed and 7-AAD stained cells evaluated by both FCM and ISS.

Based on this, we employed ISS in our further analysis to estimate the number of Oct-4$^+$/Sca-1$^+$/Lin$^-$/CD45$^-$ cells in adult organs. We noticed that a highest number of these small Oct-4$^+$ cells could be isolated from brain, kidneys, muscles, pancreas, and BM. These observations were supported by confocal microscopic analysis and RT-PCR. Thus, our data show that adult tissues may contain small, very rare Oct-4$^+$ cells. The presence of such cells in adult tissues was recently questioned, due of the existence of several Oct-4 pseudogenes and the possibility of their false positive detection. However, it is important to stress that all antibodies and primers that we employed were Oct-4 specific (27) as demonstrated in our recent work. Thus, adult tissues may contain Oct-4$^+$ cells. The presence of these cells in adult organs supports our hypothesis that early during development, primitive epiblast/germ line-related SCs may be deposited in developing tissues and organs.

ISS was a very useful method for verifying the presence of these cells and for calculating their average size and N/C ratio. We selected this technology among other approaches for quantification of cellular structure, size and volume that have been recently described (29,30). First, we noticed that Oct-4 expression correlates with Sca-1$^+$/Lin$^-$/CD45$^-$ cells that are the smallest size. Depending on the organ from which they were isolated, these Oct-4$^+$ cells were from 3 to 6 μm in diameter. In addition to BM, the smallest cells were found in murine heart and testes. Cells were slightly larger in other tissues, but their size was still smaller than or comparable to murine erythrocytes. Second, all these cells were distinguished by a high N/C ratio, which is characteristic for primitive cells. Thus, the slight differences in morphology (size, N/C ratio) between Oct-4$^+$/Sca-1$^+$/Lin$^-$/CD45$^-$cells may

depend on the niche in which they are located and perhaps could be related to their biological role within any given organ. However, this requires further study for clarification.

In conclusion, by employing flow cytometric analysis supported by ISS, confocal microscopy, and RT-PCR, we demonstrated that adult murine tissues may in fact harbor an extremely rare population of very small Oct-4^+/Sca-1^+/Lin^-/$CD45^-$ cells that correspond to pluripotent VSELs identified recently by us in murine BM. Further studies are required to show that cells identified by us in multiple tissues are similar to BM cells in their pluripotency and whether similar cells are also present in human tissues. Finally, we demonstrated the clear advantage of ISS in analyzing rare small cells isolated from homogenized tissues.

Acknowledgments

Supported by NIH grant R01 CA106281-01 and the Stella & Henry Hoenig endowment to MZR.

References

1. Kucia M, Reca R, Jala VR, Dawn B, Ratajczak J, Ratajczak MZ. Bone marrow as a home of heterogenous populations of nonhematopoietic stem cells. Leukemia. 2005; 19:1118–1127. [PubMed: 15902288]
2. Ratajczak MZ, Kucia M, Reca R, Majka M, Janowska-Wieczorek A, Ratajczak J. Stem cell plasticity revisited: CXCR4-positive cells expressing mRNA for early muscle, liver and neural cells 'hide out' in the bone marrow. Leukemia. 2004; 18:29–40. [PubMed: 14586476]
3. Asahara T, Murohara T, Sullivan A, Silver M, van der Zee R, Li T, Witzenbichler B, Schatteman G, Isner JM. Isolation of putative progenitor endothelial cells for angiogenesis. Science. 1997; 275:964–967. [PubMed: 9020076]
4. Shi Q, Rafii S, Wu MH, Wijelath ES, Yu C, Ishida A, Fujita Y, Kothari S, Mohle R, Sauvage LR, Moore MA, Storb RF, Hammond WP. Evidence for circulating bone marrow-derived endothelial cells. Blood. 1998; 92:362–367. [PubMed: 9657732]
5. Peister A, Mellad JA, Larson BL, Hall BM, Gibson LF, Prockop DJ. Adult stem cells from bone marrow (MSCs) isolated from different strains of inbred mice vary in surface epitopes, rates of proliferation, and differentiation potential. Blood. 2004; 103:1662–1668. [PubMed: 14592819]
6. Prockop DJ. Marrow stromal cells as stem cells for nonhematopoietic tissues. Science. 1997; 276:71–74. [PubMed: 9082988]
7. Jiang Y, Jahagirdar BN, Reinhardt RL, Schwartz RE, Keene CD, Ortiz-Gonzalez XR, Reyes M, Lenvik T, Lund T, Blackstad M, Du J, Aldrich S, Lisberg A, Low WC, Largaespada DA, Verfaillie CM. Pluripotency of mesenchymal stem cells derived from adult marrow. Nature. 2002; 418:41–49. [PubMed: 12077603]
8. D'Ippolito G, Diabira S, Howard GA, Menei P, Roos BA, Schiller PC. Marrow-isolated adult multilineage inducible (MIAMI) cells, a unique population of postnatal young and old human cells with extensive expansion and differentiation potential. J Cell Sci. 2004; 117:2971–2981. [PubMed: 15173316]
9. Johnson J, Bagley J, Skaznik-Wikiel M, Lee HJ, Adams GB, Niikura Y, Tschudy KS, Tilly JC, Cortes ML, Forkert R, Spitzer T, Iacomini J, Scadden DT, Tilly JL. Oocyte generation in adult mammalian ovaries by putative germ cells in bone marrow and peripheral blood. Cell. 2005; 122:303–315. [PubMed: 16051153]
10. Nayernia K, Lee JH, Drusenheimer N, Nolte J, Wulf G, Dressel R, Gromoll J, Engel W. Derivation of male germ cells from bone marrow stem cells. Lab Invest. 2006; 86:654–663. [PubMed: 16652109]
11. Kucia M, Reca R, Campbell FR, Zuba-Surma E, Majka M, Ratajczak J, Ratajczak MZ. A population of very small embryonic-like (VSEL) CXCR4(+)SSEA-1(+)Oct-4+ stem cells identified in adult bone marrow. Leukemia. 2006; 20:857–869. [PubMed: 16498386]

12. Zuba-Surma EK, Kucia M, Abdel-Latif A, Dawnn B, Hall B, Singh R, Lillard JW, Ratajczak MZ. Morphological characterization of Very Small Embryonic-Like stem cells (VSELs) by ImageStream system analysis. J Cell Mol Med. 2008; 12:292–303. [PubMed: 18031297]
13. Wojakowski W, Kucia M, Zuba-Surma E, Ratajczak J, Machalinski B, Tendera M, Ratajczak MZ. Cardiogenic differentiation of very small embryonic-like cells isolated from adult bone marrow. J Am Col Cardiol. 2007; 49:83A.
14. Zuba-Surma EK, Abdel-Latif A, Tiwari S, Khayat M, Bolli R, Dawn B. Antigenically-defined subsets of bone marrow mesenchymal stem cells exhibit differential cardionnyogenic and angiogenic potential. Circulation. 2006; 114:170.
15. Kucia M, Wu W, Ratajczak MZ. Bone marrow-derived very small embryonic-like stem cells: Their developmental origin and biological significance. Dev Dyn. 2007; 12:3309–3320. [PubMed: 17497671]
16. Ratajczak MZ, Machalinski B, Wojakowski W, Ratajczak J, Kucia M. A hypothesis for an embryonic origin of pluripotent Oct-4+ stem cells in adult bone marrow and other tissues. Leukemia. 2007; 21:860–867. [PubMed: 17344915]
17. Howell JC, Lee WH, Morrison P, Zhong J, Yoder MC, Srour EF. Pluripotent stem cells identified in multiple murine tissues. Ann N Y Acad Sci. 2003; 996:158–173. [PubMed: 12799294]
18. Jones RJ, Wagner JE, Celano P, Zicha MS, Sharkis SJ. Separation of pluripotent haematopoietic stem cells from spleen colony-forming cells. Nature. 1990; 347:188–189. [PubMed: 2395470]
19. Vacanti MP, Roy A, Cortiella J, Bonassar L, Vacanti CA. Identification and initial characterization of spore-like cells in adult mammals. J Cell Biochem. 2001; 80:455–460. [PubMed: 11135375]
20. Zuba Surma E, Kucia M, Ratajczak J, Ratajczak M. “Small Stem Cells” in Adult Tissues: Very Small Embryonic-Like Stem Cells (VSELs) Stand Up! Cytometry A. 2008 in press.
21. Li Y, Atmaca-Sonmez P, Schanie CL, Ildstad ST, Kaplan HJ, Enzmann V. Endogenous Bone Marrow Derived Cells Express Retinal Pigment Epithelium Cell Markers and Migrate to Focal Areas of RPE Damage. Invest Ophthalmol Vis Sci. 2007; 48:4321–4327. [PubMed: 17724223]
22. Trujillo C, Schwindt T, Martins A, Alves J, Mello L, Ulrich H. Novel perspectives of neural stem cell differentiation: from neurotransmitters to therapeutics. Cytometry A. 2008 in press.
23. Zuba-Surma E, Kucia M, Ratajczak J, Ratajczak M. “Small Stem Cells” in Adult Tissues: Very Small Embryonic-Like Stem Cells (VSELs) Stand Up! Cytometry A. 2008 in press.
24. George TC, Basiji DA, Hall B, Lynch DH, Ortyn WE, Perry DJ, Seo MJ, Zimmerman CA, Morrissey PJ. Distinguishing Modes of Cell Death Using the ImageStream Multispectral Imaging Flow Cytometer. Cytometry A. 2004; 59A:237–245. [PubMed: 15170603]
25. George TC, Fanning SL, Fitzgeral-Bocarsly P, Medeiros RB, Highfill S, Shimizu Y, Hall BE, Frost K, Basiji D, Ortyn WE, Morrissey PJ, Lynch DH. Quantitative measurement of nuclear translocation events using similarity analysis of multispectral cellular images obtained in flow. J Immunol Methods. 2006; 311:117–129. [PubMed: 16563425]
26. Ortyn WE, Hall BE, George TC, Frost K, Basiji DA, Perry DJ, Zimmerman CA, Coder DC, Morrissey PJ. Sensitivity Measurement and Compensation in Spectral Imaging. Cytometry A. 2006; 69A:852–862. [PubMed: 16969805]
27. Kucia M, Wysoczynski M, Wu W, Zuba-Surma EK, Ratajczak J, Ratajczak MZ. Evidence that Very Small Embryonic Like (VSEL) Stem Cells are Mobilized into Peripheral Blood. Stem Cells. 2008; 26:2083–2092. [PubMed: 18511604]
28. Zuba-Surma EK, Kucia M, Dawn B, Guo Y, Ratajczak MZ, Bolli R. Bone marrow-derived pluripotent very small embryonic-like stem cells (VSELs) are mobilized after acute myocardial infarction. J Mol Cell Cardiol. 2008; 44:865–873. [PubMed: 18430437]
29. Sharma S, Cabana R, Shariatmadar S, Krishan A. Cellular volume and marker expression in human peripheral blood apheresis stem cells. Cytometry A. 2008; 73:160–167. [PubMed: 18189285]
30. Rajwa B, Venkatapathi M, Ragheb K, Banada PP, Hirleman ED, Lary T, Robinson JP. Automated classification of bacterial particles in flow by multiangle scatter measurement and support vector machine classifier. Cytometry A. 2008; 73:369–379. [PubMed: 18163466]

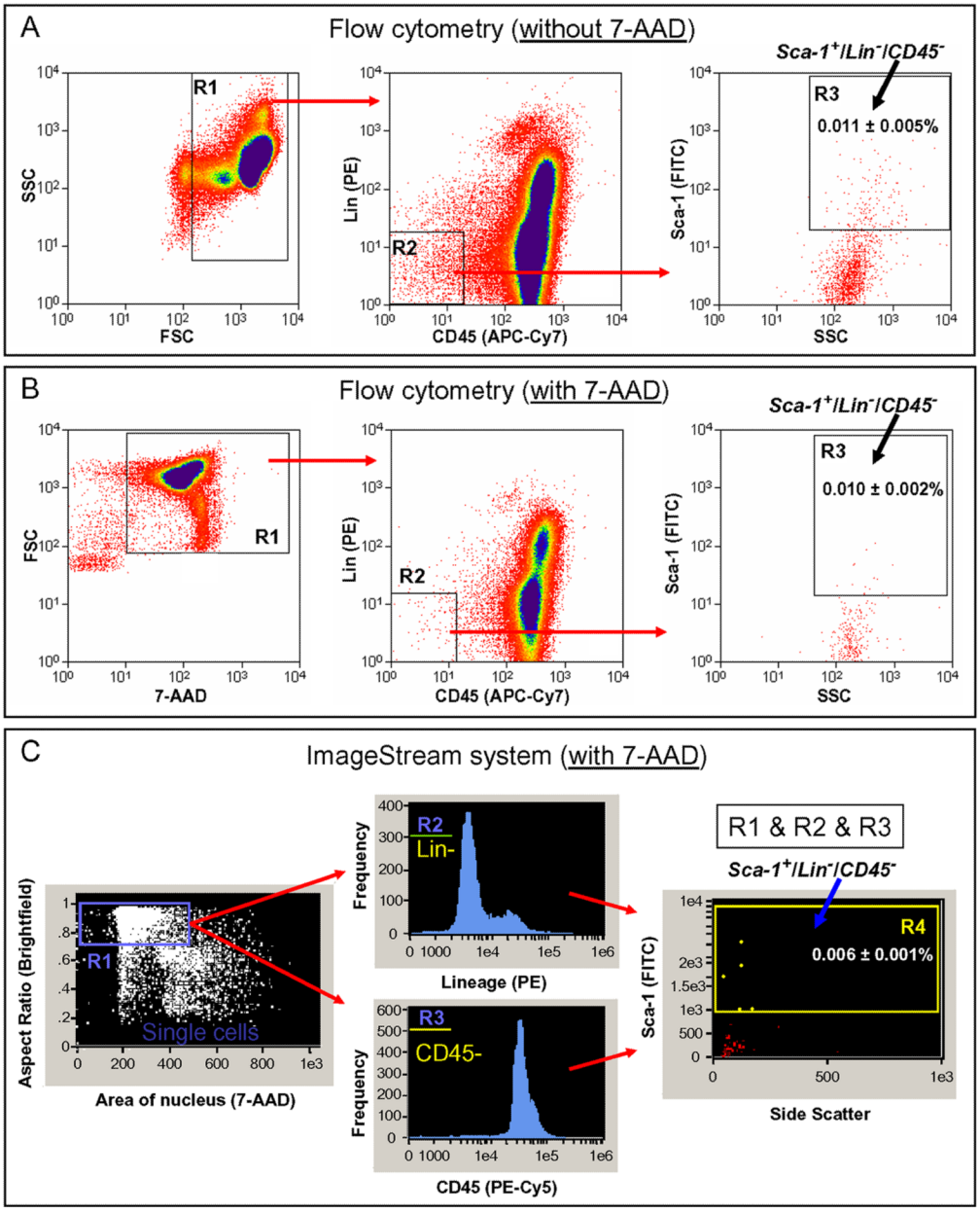

Figure 1. Flow cytometric and ISS analyses of cells isolated from murine organs

The schemes of analyses are based on a sample of cells isolated from thymus. Cells were stained with antibodies against CD45, Lin, and Sca-1 (BD Pharmingen) and freshly analyzed by MoFlo cell sorter (Dako) (**Panel A**) or fixed with 4% paraformaldehyde and stained with 7-AAD (Invitrogen; 40μm) for further flow cytometric analysis with MoFlo (**Panel B**) and ISS 100 (Amnis Corp.) (**Panel C**). **Panel A** shows flow cytometric analysis of cells without 7-AAD. Cells are presented on cytogram of FSC vs. SSC characteristics. Region R1 encloses all objects larger than 2μm in size that have been estimated when compared with size-predefined beads (Flow Cytometry Size beads, Invitrogen; Molecular Probes). Cells from Region R1 were further analyzed for CD45 and hematopoietic Lin expression. $Lin^-/CD45^-$ cells included in Region R2 are visualized based on their SSC characteristics and Sca-1 expression. Region R3 includes cells that are $Sca\text{-}1^+/Lin^-/CD45^-$.

Panel B shows the cytogram of FSC characteristics of fixed cells and their staining for 7-AAD. Only events exhibiting DNA content are included in Region R1. 7-AAD$^+$ events are visualized based on their CD45 vs. Lin expression and Lin$^-$/CD45$^-$ objects are included in Region R2. Cells from Region R2 are analyzed based on their SSC characteristics as well as their Sca-1 expression. Region R3 encloses Sca-1$^+$/Lin$^-$/CD45$^-$ cells. **Panel C** presents ISS analysis of fixed cells in the presence of 7-AAD. The first plot shows objects according to their morphological parameters including the area of the nucleus and the aspect ratio of brightfield. The aspect ratio is calculated based on brightfield as the ratio of cellular minor axis (width) to major axis (height). Round, non-elongated cells have an aspect ratio close to 1.0, while the elongated cells or clumps had a lower aspect ratio. We included round, single cells containing DNA for further analysis (Region R1). Objects from Region R1 are visualized based on the expression of CD45 and Lin (middle histograms). Lin$^-$/CD45$^-$ objects from Regions R2 and R3 are visualized on the dot-plot presenting their side scatter characteristics and Sca-1 expression. Sca-1$^+$/Lin$^-$/CD45$^-$ cells are included in Region R4. Percentages on all panels represent the content of Sca-1$^+$/Lin$^-$/CD45$^-$ cells among total cells derived from the thymus that were estimated with both methods (Mean± SEM).

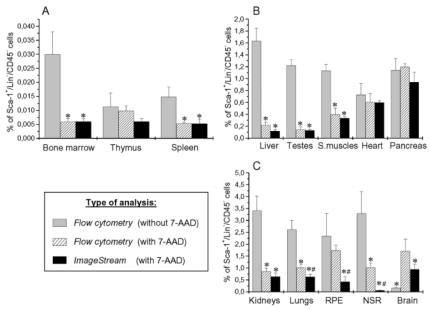

Figure 2. Percent content of Sca-1^{+}/Lin^{-}/CD45^{-} cells in murine organs by flow cytometry and ISS

Cells isolated from organs of adult (4-8 week old) C57BL/6 mice were stained against CD45, Lin, and Sca-1. Cells were analyzed by MoFlo flow cytometer and ISS as described in Figure 1. Gray bars represent the percent content of Sca-1^{+}/Lin^{-}/CD45^{-} cells estimated by flow cytometry without 7-AAD, while hatched bars and black bars show the results obtained by flow cytometry and ISS with 7-AAD, respectively (**Panels A-C**). Results are presented as Mean ± SEM. Statistically significant differences ($P<0.05$) are shown when compared to: (*) results by flow cytometry without 7-AAD and (#) results by ISS obtained for each organ. Analysis was performed three times (N=3) with samples prepared from three independent organs for each analysis.

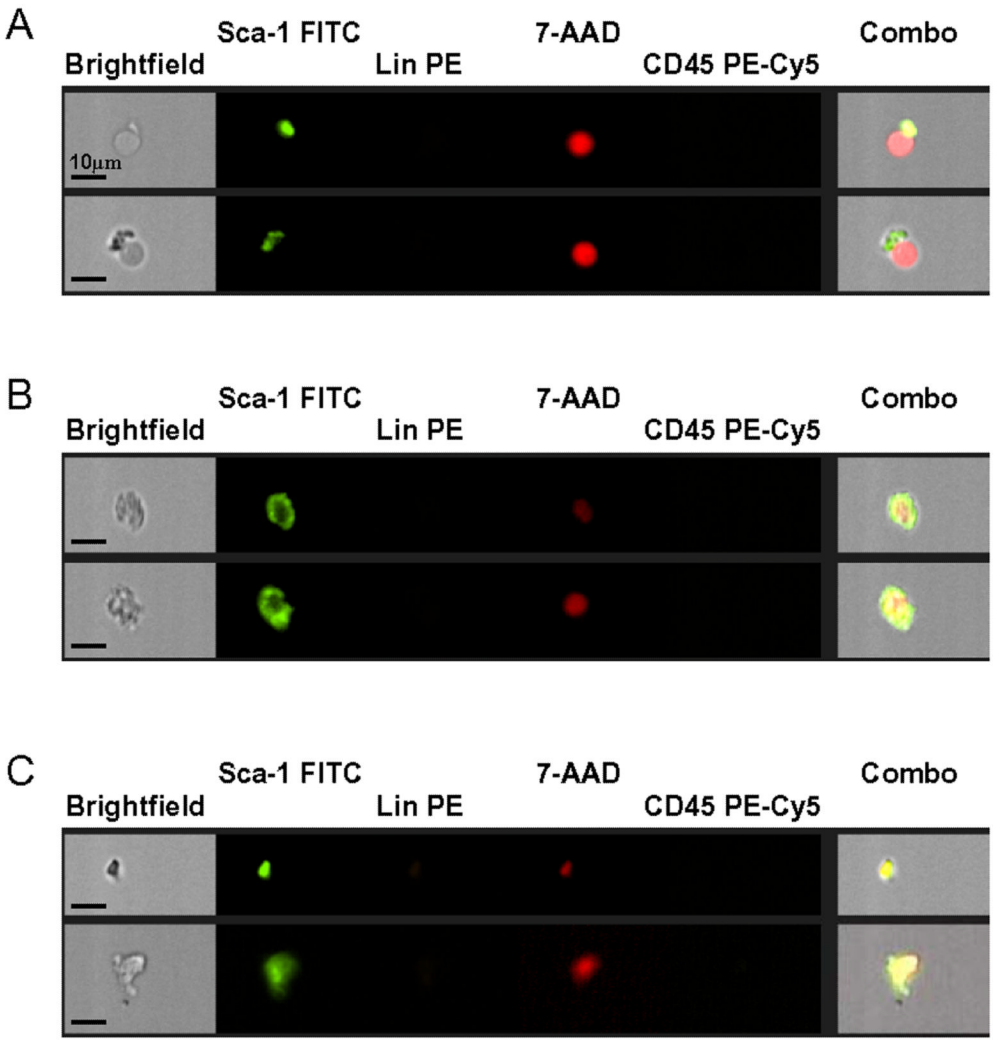

Figure 3. Artifacts detected with ISS

Selected images of falsely "positive" artifacts (**Panel A**), damaged/ degradating cells (**Panel B**), and cellular debris (**Panel C**) are shown. Each photograph presents brightfield image, separate fluorescent images related to nuclear image (7-AAD; red), and expression of Sca-1 (FITC, green), Lin (PE; orange), and CD45 (PE-Cy5; yellow) as well as a composite image combining brightfield, 7-AAD, and Sca-1 images. The scale bar indicates 10μm.

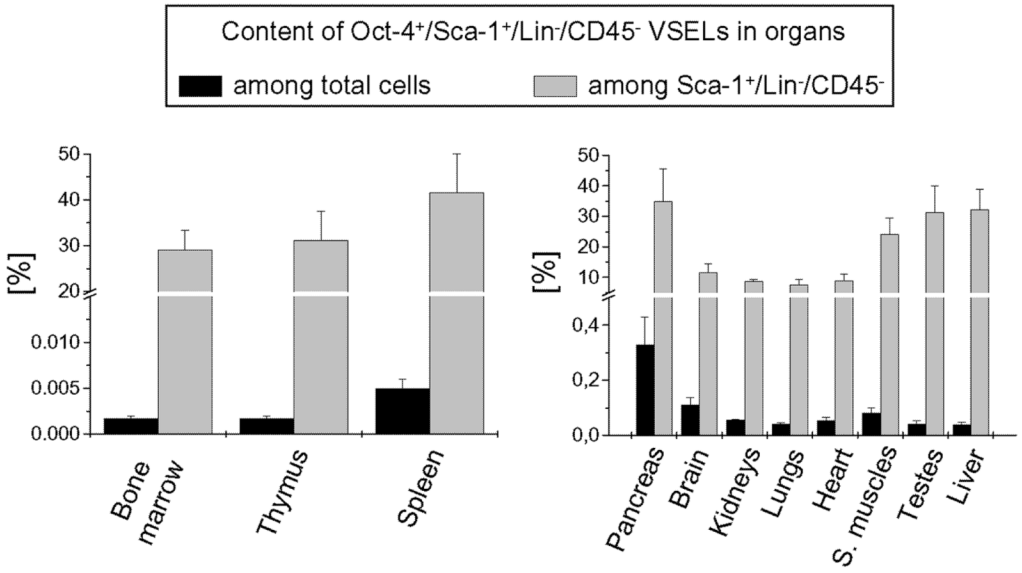

Figure 4. Percent content of Oct-4^{+}/Sca-1^{+}/Lin^{-}/CD45^{-} cells in murine organs by ISS

Cells isolated from organs of adult (4-8 week old) C57BL/6 mice were stained for Oct-4, CD45, Lin, and Sca-1. Cells were analyzed by ISS to detect intranuclear expression of Oct-4. Black bars show the percent content of Oct-4^{+} VSELs among total cells isolated from each organ, while gray bars show the content of these cells in the fraction of Sca-1^{+}/Lin^{-}/CD45^{-} cells. Results are presented as Mean ± SD. Analysis was performed three times (N=3) with samples prepared from three independent organs for each analysis.

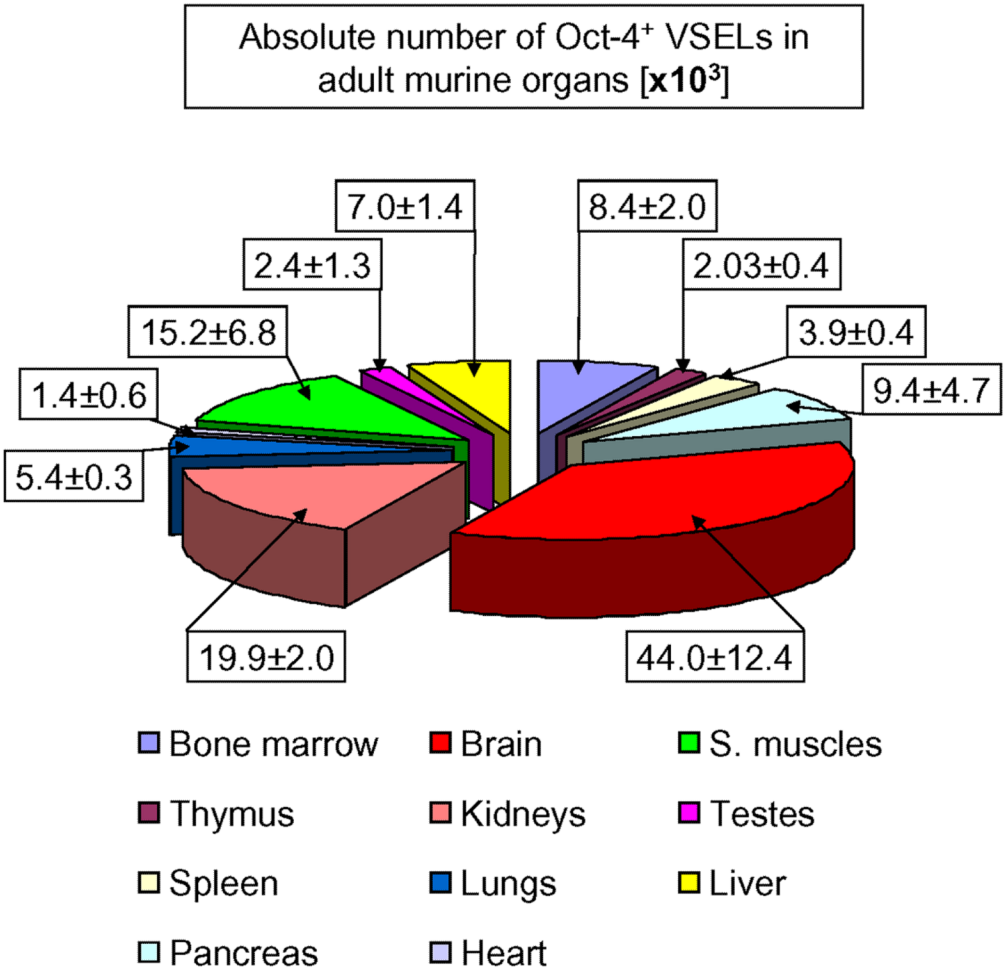

Figure 5. Absolute numbers of Oct-4$^+$/Sca-1$^+$/Lin$^-$/CD45$^-$ cells present in murine organs

The content of Oct-4$^+$ VSELs calculated per organ [×10^3] by employing percent content obtained by ISS and total numbers of cells isolated from each organ are shown. Values are presented as Mean ± SEM. The percentages are related to the total number of Oct-4$^+$ cells per mouse and computed as the sum of these cells detected in all analyzed organs. Analysis was performed three times (N=3) with samples prepared from three independent organs for each analysis.

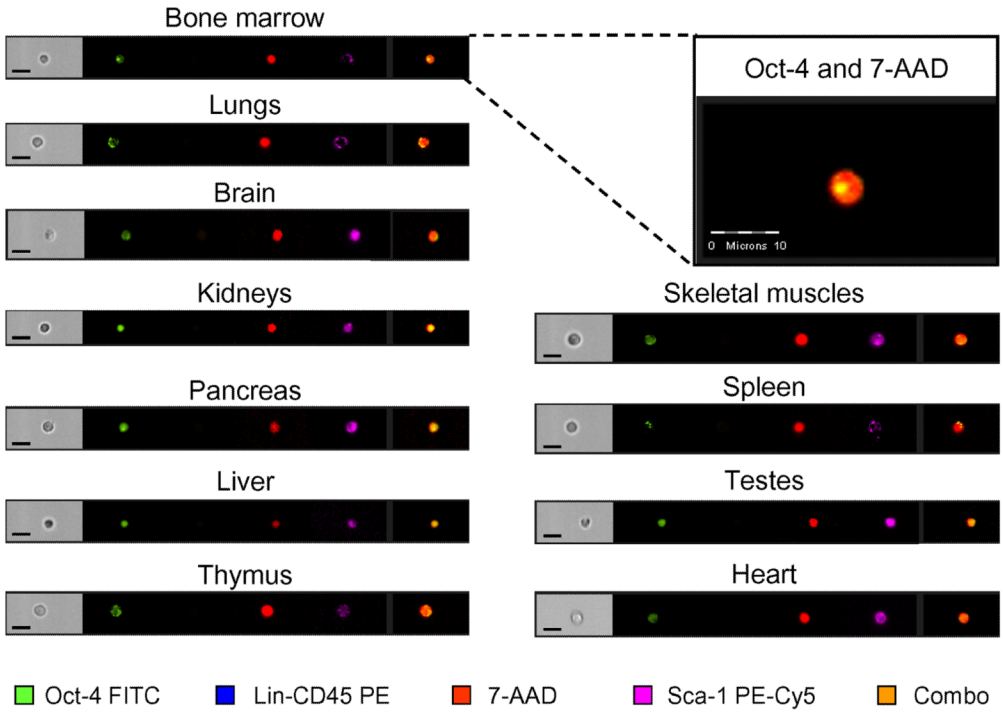

Figure 6. Representative images of Oct-4^{+}/Sca-1^{+}/Lin^{-}/CD45^{-} cells detected in murine organs by ISS

Cells isolated from organs were stained for pluripotent marker, Oct-4 (FITC; green), CD45 and Lin (PE; orange), and Sca-1 (PE-Cy5; magenta). Cells were stained with 7-AAD (red) to visualize nuclei and analyzed by ISS to detect intranuclear expression of Oct-4 as shown in magnified, combined images. The scale bars indicate 10μm.

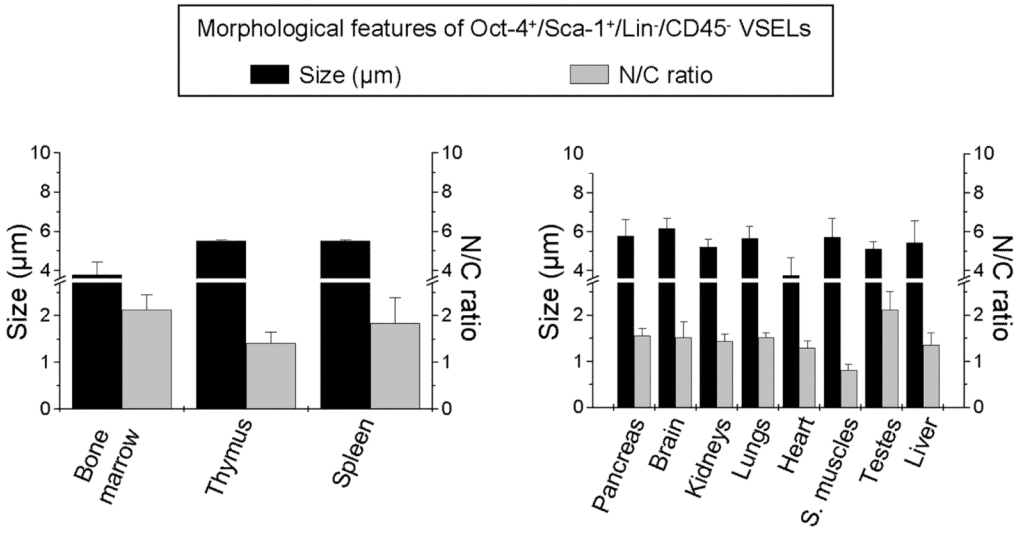

Figure 7. Morphology of Oct-4$^+$/Sca-1$^+$/Lin$^-$/CD45$^-$ cells present in murine organs by ISS

Cells isolated from organs were stained for pluripotent marker Oct-4, CD45, Lin, and Sca-1. Oct-4+ VSELs were identified by ISS as Sca-1$^+$/Lin$^-$/CD45$^-$ cells with intranuclear expression of Oct-4. Morphological features of cells such as size and N/C ratio were calculated using images of cells by IDEAS software. Size (black bars) was calculated based on brightfield images of cells as a length of the minor cellular axis expressed in micrometers, while N/C ratio (gray bars) was computed based on brightfield cellular images and nuclear images as a ratio between the area of the cytoplasm and the area of the nucleus. Results are presented as Mean ± SD. Analysis was performed three times (N=3) with samples prepared from three independent organs for each analysis.

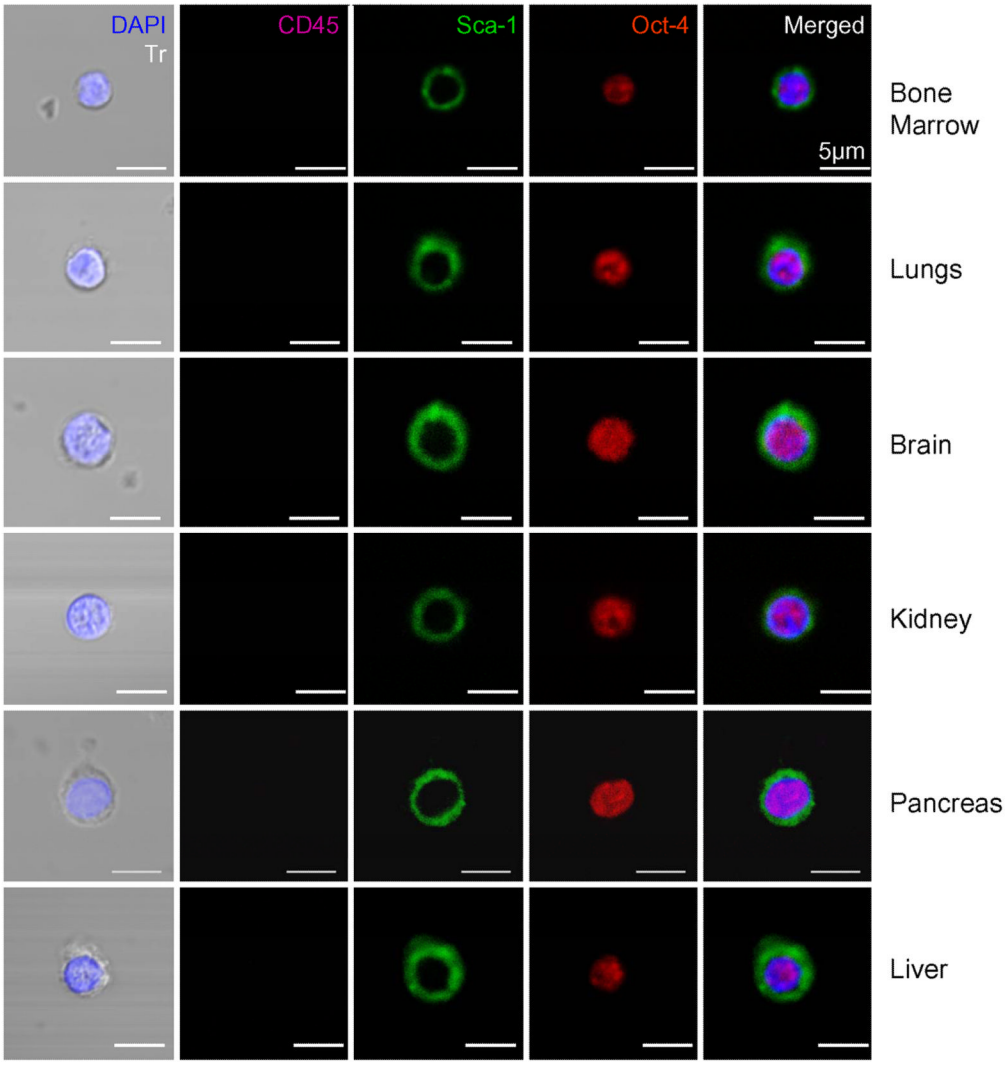

Figure 8. Confocal microscopic images of Oct-4+ VSELs detected in adult organs

Sorted Sca-1^{+}/Lin^{-}/CD45^{-} cells were stained for Oct-4 (TRITC; red), CD45 (Cy5; magenta), and Sca-1 (FITC; green). Nuclei were stained with DAPI (blue). Representative images show Oct-4^{+}/Sca-1^{+}/Lin^{-}/CD45^{-} cells (VSELs) that are negative for CD45 and positive for Oct-4, which is a marker of pluripotent cells and Sca-1. Merged images show intranuclear staining for Oct-4 and surface appearance of Sca-1 antigen. The scale bars indicate 5μm.

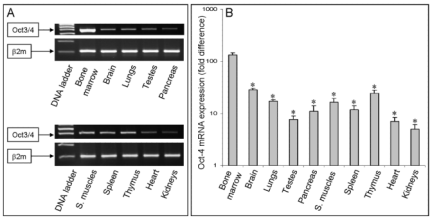

Figure 9. Expression of mRNA for Oct-4 in cells isolated from murine organs

Panel A shows the expression of mRNA for Oct-4 and β2-microglobulin in sorted Sca-1^{+}/Lin^{-}/$CD45^{-}$ cells derived from each organ and investigated by RT-PCR. **Panel B** presents the expression of Oct-4 by real time RT-PCR in the sorted fractions. The graph shows the fold difference in the concentration of mRNA for Oct-4 between the organs when compared to the lowest expression detected in liver (not shown; recalculated as 1). Results are presented as Mean ± SEM. Statistically significant differences (*; $P<0.05$) are shown when compared to liver. Analysis was performed three times (N=3) with samples prepared from three independent organs for each analysis.

Table 1

Content and morphological features of Sca-1$^+$/Lin$^-$/CD45$^-$ cells in adult murine organs and tissues by ISS. Cells were isolated from tissues of adult 4-8 week old mice (C57BL/6) by enzymatic digestion. Analysis was performed three times (N=3) on samples prepared from organs of three independent animals. (*) In case of geminate organs, the absolute numbers of cells were calculated per one animal.

Organ/Tissue:	Content of Sca-1$^+$/Lin$^-$/CD45$^-$cells [%]	Content of cells <6μm [%]	Absolute number of Sca-1$^+$/Lin$^-$/CD45$^-$cells [10^3]		Morphological features of Sca-1$^+$/Lin$^-$/CD45$^-$cells	
	Among total cells	Among Sca-1$^+$/Lin$^-$/CD45$^-$cells	per organ (*)	per 1g of tissue	Size [μm]	N/C ratio
	Mean±SEM	Mean±SEM	Mean±SEM	Mean±SEM	Mean±SD	Mean±SD
Bone marrow	0.006±0.001	93.45±6.55	27.96±6.68	36.37±8.69	3.63±0.27	1.47±0.17
Thymus	0.006±0.001	41.4±8.60	6.76±1.22	81.48±14.74	5.40±1.13	1.41±0.02
Spleen	0.005±0.002	45.3±4.70	3.86±0.43	47.10±5.21	6.81±0.09	1.51±0.02
Pancreas	0.943±0.166	35.15±10.46	26.90±13.47	78.66±39.37	7.67±0.08	0.91±0.04
Brain	0.947±0.215	21.33±7.38	378.52±106.60	998.72±281.26	7.20±0.14	1.24±0.11
Kidneys	0.644±0.149	9.01±1.71	228.50±23.30	530.15±54.07	7.28±0.11	1.30±0.09
Lungs	0.633±0.108	19.38±2.98	81.22±4.93	514.04±31.19	6.69±0.13	1.41±0.15
Heart	0.599±0.030	13.59±2.52	14.98±6.23	110.11±45.83	6.90±0.29	1.01±0.14
Skeletal m.	0.339±0.018	18.85±7.25	62.78±28.06	17.20±7.69	7.09±0.28	1.07±0.11
Testes	0.131±0.018	26.65±16.55	7.59±4.01	30.50±16.10	7.83±0.32	2.07±0.30
Liver	0.120±0.021	17.65±1.75	21.47±4.25	14.74±2.92	8.40±0.17	0.91±0.10
RPE	0.422±0.213	2.65±1.55	3.17 ±1.06	nd	6.83±0.45	0.84±0.19
NSR	0.061±0.016	17,10±4.40	2.14±0.31	nd	6.66±0.21	1.11±0.15

Table 2

Content and morphological features of Oct-4$^+$/Sca-1$^+$/Lin$^-$/CD45$^-$ cells in adult murine organs and tissues by ISS. Cells were isolated from tissues of adult 4-8 week old mice (C57BL/6) by enzymatic digestion. Analysis was performed three times (N=3) on samples prepared from organs of three independent animals. (*) In case of geminate organs, the absolute numbers of cells were calculated per one animal.

Organ/Tissue:	Content of Oct-4$^+$VSELs [%]		Content of cells <6μm [%]	Absolute number of Oct-4$^+$ VSELs [10^3]		Morphological features of Oct-4$^+$ VSELs	
	Among total cells	Among Sca-1$^+$/Lin$^-$/CD45$^-$cells	Among Oct-4$^+$ VSELs [%]	per organ (*)	per 1g of tissue	Size [μm]	N/C ratio
	Mean±SEM	Mean±SEM	Mean±SEM	Mean±SEM	Mean±SEM	Mean±SD	Mean±SD
Bone marrow	0.0018±0.0003	29.15±4.15	100.00±0.00	8.39±2.00	10.91±2.61	3.78±0.64	2.12±0.33
Thymus	0.0018±0.0003	31.25±6.25	90.00±10.00	2.03±0.37	24.44±4.42	5.50±0.05	1.41±0.23
Spleen	0.005±0.001	41.65±8.35	89.50±9.50	3.86±0.43	47.10±5.21	5.50±0.06	1.83±0.56
Pancreas	0.330±0.099	34.98±10.48	75.00±5.00	9.41±4.71	27.53±13.78	5.77±0.83	1.56±0.14
Brain	0.110±0.027	11.64±2.84	62.13±19.61	43.97±12.38	116.01±32.67	6.16±0.51	1.52±0.33
Kidneys	0.056±0.004	8.67±0.57	78.25±1.75	19.87±2.03	46.10±4.70	5.21±0.40	1.44±0.15
Lungs	0.042±0.004	7.62±1.62	51.65±18.35	5.39±0.33	34.11±2.07	5.66±0.60	1.52±0.10
Heart	0.054±0.013	8.95±2.15	91.62±10.04	1.35±0.56	9.93±4.13	4.74±0.93	1.39±0.15
Skeletal m.	0.082±0.018	24.17±5.27	64.50±4.50	15.18±6.79	4.16±1.86	5.72±0.97	0.81±0.12
Testes	0.041±0.011	31.46±8.56	100.00±0.00	2.38±1.25	9.55±10.04	5.11±0.36	2.11±0.40
Liver	0.039±0.008	32.33±6.53	63.55±6.45	6.98±1.38	4.79±0.95	5.45±1.12	1.35±0.27